(10) J. A. Pople, D. L. Beveridge, and P. A. Dobosh, *J. Am. Chem. Soc.*, **90**, 7142 (1968); J. A. Pople and D. L. Beveridge, "Approximate Molecular Orbital Theory", McGraw-Hill, New York, N.Y., 1970.
(11) A. T. Casey, R. A. Craig, and M. J. Scarlett, *J. Chem. Soc., Faraday Trans. 2*, **69**, 132 (1973).
(12) We used the representations of C_{2v} to maintain the flow of discussion for the radical anions. See Figure 5 for corresponding representations.
(13) C. R. Brundle, M. B. Robin, and N. A. Kuebler, *J. Am. Chem. Soc.*, **94**, 1466, 1451 (1972); M. B. Robin, "Higher States of Polyatomic Molecules," Vol. II, Academic Press, New York, N.Y., 1975, and references cited therein.
(14) I. Nenner and G. J. Schulz, *J. Chem. Phys.*, **62**, 1747 (1975).
(15) M. Shiotani and F. Williams, *J. Am. Chem. Soc.*, **98**, 4006 (1976).
(16) M. Shiotani and F. Williams, private communication.

Excited Potential Energy Hypersurfaces for H_4. 2. "Triply Right" (C_{2v}) Tetrahedral Geometries. A Possible Relation to Photochemical "Cross-Bonding" Processes

Wolfgang Gerhartz,[1a,b] Ronald D. Poshusta,*[1c] and Josef Michl*[1b]

Contribution from the Department of Chemistry, University of Utah, Salt Lake City, Utah 84112, and the Chemical Physics Program, Washington State University, Pullman, Washington 99163. *Received November 3, 1976*

Abstract: Ab initio VB calculations, complete within minimum basis set (STO-4G), were performed on the Born–Oppenheimer potential surfaces of the four lowest singlet electronic states of the H_4 molecule for the three-dimensional subspace of "triply right" (C_{2v}) tetrahedra. Perspective drawings of equipotential surfaces aid the visualization of the results, which include some multidimensional funnels. The results suggest a path for the known efficient quenching of $H_2(B^1\Sigma_u^+)$ by $H_2(X^1\Sigma_g^+)$ and propensity for diagonal bonding in the lowest excited singlet state in $4N$-pericyclic arrays in general, and this may be of importance for some organic photochemical mechanisms.

A previous paper in this series,[2] hereafter called part I, presented results for potential energy hypersurfaces of H_4 in the three-dimensional subspace of all trapezoids, and discussed their relation to 2s + 2s photochemical processes. In the present paper we describe results for the four lowest singlet states in a three-dimensional subspace of all "triply right" C_{2v} tetrahedra (defined below) and discuss their implications for the presently poorly understood molecular photochemistry of H_2 and for the understanding of "cross-bonding" in photochemical reactions in general.

Method of Calculation

The MB method of calculation (minimum basis set separately optimized for each state and each geometry, full configuration interaction) and the manner of presenting the results are the same as in part I,[2] which also discusses the accuracy and limitations inherent in the approach.

The geometries of H_4 presently considered are defined in Figure 1. The nuclei are labeled A, B, C, and D. The distance between A and B is denoted by $R_1 = \overline{AB}$, that between C and D by $R_2 = \overline{CD}$, and the distance between the midpoints of the lines AB and CD is labeled R. The axis connecting these midpoints is referred to as z and is perpendicular to both AB and CD, $\theta_1 = \theta_2 = 90°$. The dihedral angle, α, defined by the plane containing AB and z and that containing CD and z, is 90°. In this sense, then, the tetrahedra, ABCD, are triply right. in general, they belong to the C_{2v} point group. If $R_1 = R_2$, $R \neq 0$ and $R \neq R_1/\sqrt{2}$ the symmetry group is D_{2d}; if $R_1 \neq R_2$ and $R = 0$, the symmetry is D_{2h}; if $R_1 = R_2$ and $R = 0$, the symmetry is D_{4h}, and if $R_1 = R_2$, $R = R_1/\sqrt{2}$, the symmetry is T_d. Since the square (D_{4h}) geometries are special instances of trapezoidal geometries, they were already considered in part I, and provide an interface between the two sets of results.

When $R_1 \neq R_2$, the nuclei A and B are not equivalent to nuclei C and D. Therefore, their respective orbital exponents are not required by symmetry to be equal and were allowed to optimize to different values. Even when $R_1 = R_2$ (D_{2d}, D_{4h}, and T_d) at which all nuclei are equivalent, lower energies are frequently obtained by allowing "symmetry breaking" in the wave function, i.e., permitting the exponents of A and B orbitals to be different from those of C and D orbitals. This freedom was allowed throughout, since discontinuities in potential energy surfaces would otherwise result. The resulting wave functions do not always possess irreducible symmetry of the D_{2d}, D_{4h}, or T_d group. (See the Discussion for more detail.)

Graphical Presentation

The results to be displayed are potential energy hypersurfaces. Since four dimensions would be required to plot $E(R_1R_2R)$, we present instead a three-dimensional analogy to the well-known contour diagrams. For a given electronic state, we show a series of nested equipotential surfaces, each labeled by its energy in atomic units (Figures 2–5). The energy values at specific geometries cannot be read with great accuracy from the figures. But, then, there would be little point in a very accurate display of rather approximate results, except as a benchmark for future comparison with more accurate results, which will probably be done at selected points only. The surfaces are only approximate because of the limited nature of the basis set discussed in part I,[2] and because the grid used for their construction was relatively sparse, particularly in regions which appeared to be smooth or of little interest, in line with the general philosophy adopted (about 300 points for each state). The main purpose is to display low-energy reaction paths, minima, barriers, and avoided crossings and we believe that all such features shown in Figures 2–5 are semiquantitatively reliable. Details of slopes and absolute energy differences between surfaces of differing degrees of ionicity are not reliable, particularly those of the excited singlets.

The coordinate system for plotting the isoenergetic surfaces as a function of R_1, R_2, and R is the same as in Figure 7 of part

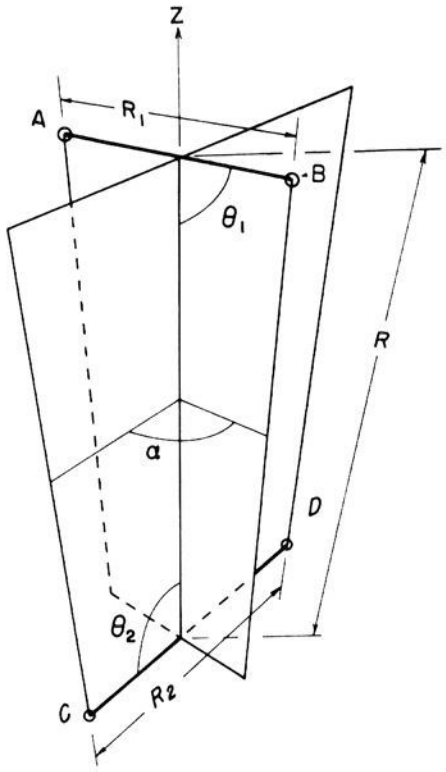

Figure 1. The coordinate system and molecular parameters for tetrahedral H_4. Triply right tetrahedra have $\theta_1 = \theta_2 = \alpha = 90°$.

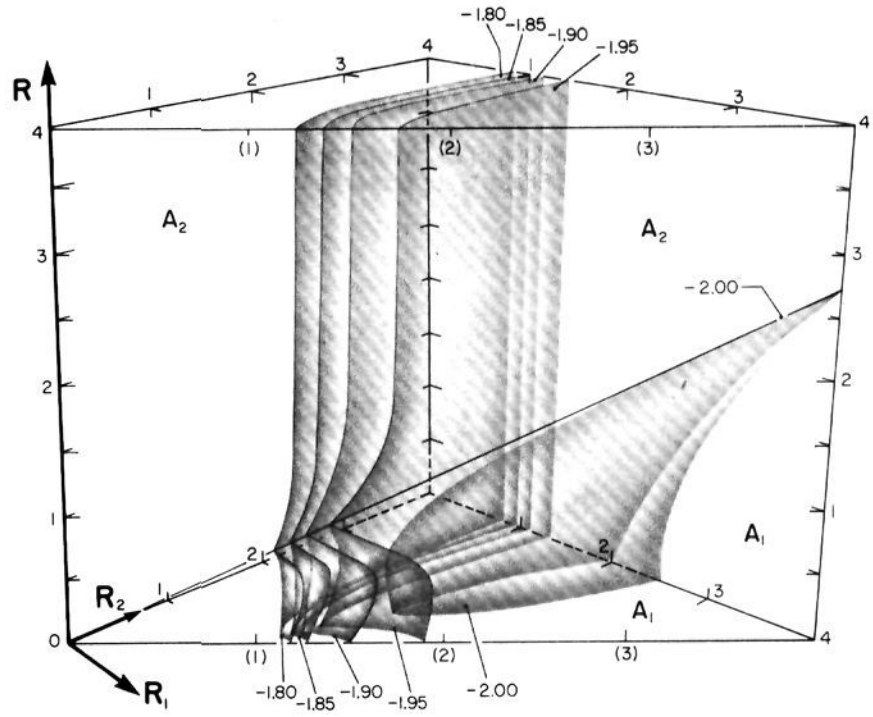

Figure 3. The first excited singlet, S_1, potential energy hypersurfaces of triply right tetrahedral H_4.

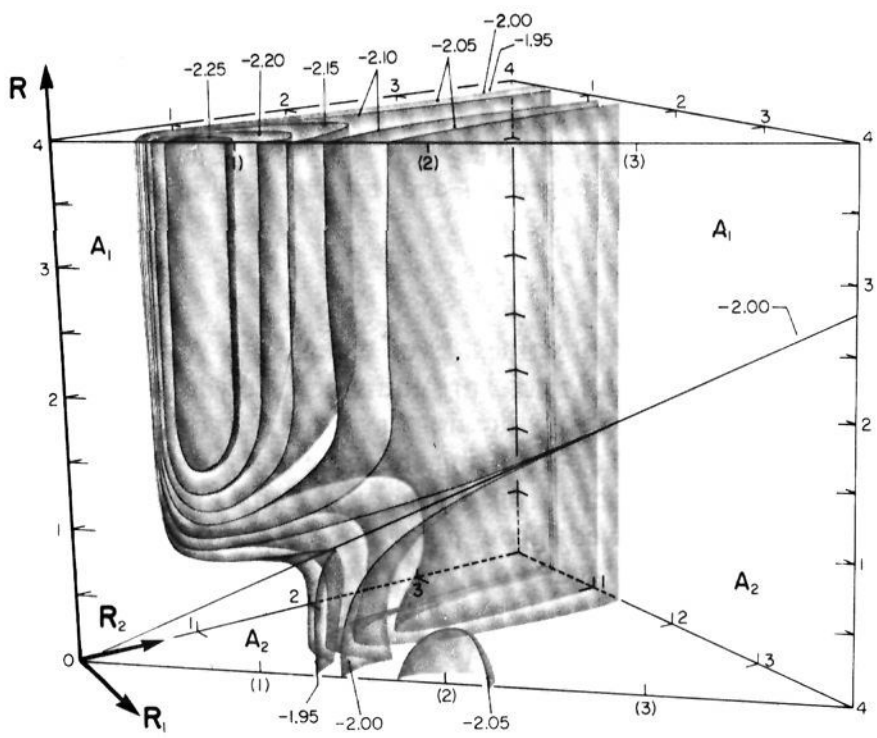

Figure 2. The lowest singlet, S_0, potential energy hypersurfaces of triply right tetrahedral H_4. Energies are given in atomic units (au) and distances in angstroms (Å).

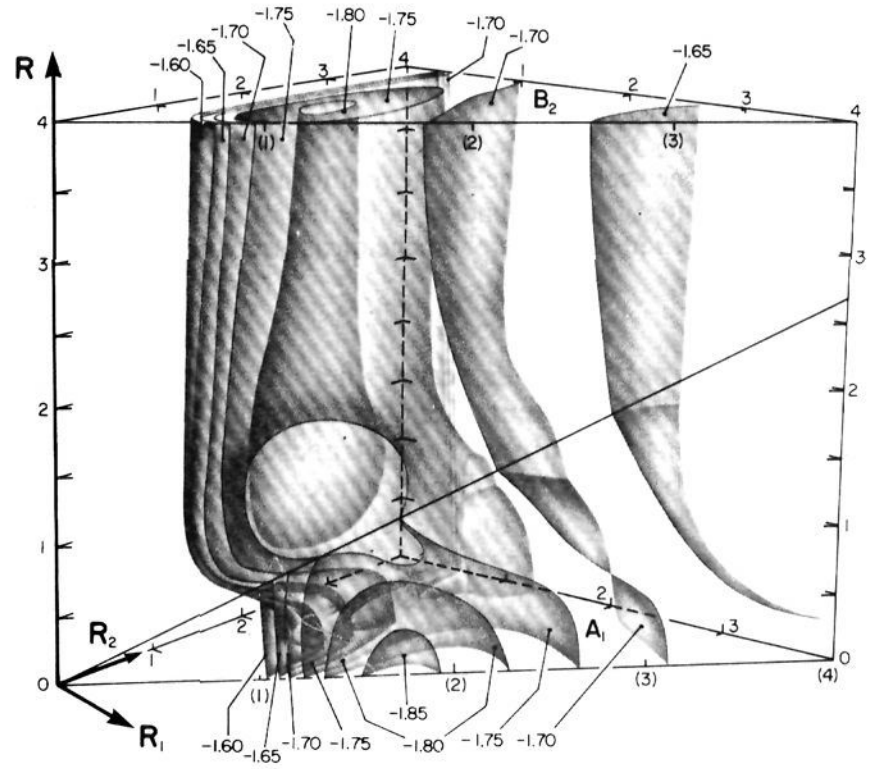

Figure 4. The second excited singlet, S_2, potential energy hypersurfaces of triply right tetrahedral H_4.

I:[2] the present figures display a prism in the first octant of the R_1, R_2, R cartesian system defined by the relations R_1, R_2, $R \geq 0$; $R_2 \geq R_1$; R, $R_2 \leq 4$ Å. Of course, the significance of the coordinates is now different from what it was in part I. In general, a point in the prism corresponds to a C_{2v} tetrahedron of Figure 1. Each point in the $R = 0$ plane corresponds to a rhombus (D_{2h}). Further, points on the $R = 0$, $R_1 = R_2$ line correspond to a square (D_{4h}), and motion of a point away from this line in the $R = 0$ plane corresponds to distorting the square into an increasingly acute rhombus. Each point in the $R_1 = R_2$ plane corresponds to a D_{2d} tetrahedron, which can be envisaged as two equivalent H_2 molecules in "perpendicular" approach. At any point on the $R_1 = R_2 = R\sqrt{2}$ line shown in Figures 2–5, the distance of the two molecules is such that the tetrahedron is regular (T_d). Motion of a point away from the regular tetrahedra line, but within the $R_1 = R_2$ plane either elongates ($R > R_1/\sqrt{2}$) or shortens ($R < R_1/\sqrt{2}$) the tetrahedron, keeping the ends AB and CD equivalent. Motion of a point away from the $R_1 = R_2$ plane corresponds to making the length of the ends AB and CD unequal, but maintaining them perpendicular. The planes $R_1 = 0$ and $R_2 = 0$ correspond to coincidence of two nuclei; no energy surfaces intersect these planes. Both of these planes as well as the $R = 0$ and $R_1 = R_2$ planes are mirror image symmetry planes. Therefore, the portion displayed in Figures 2–5 permits visualization of the energy surfaces throughout the space within -4 Å $\leq R_1, R_2, R \leq 4$ Å.

The coordinate system R_1, R_2, R determines all possible triply right tetrahedra as described above. Two other triply right tetrahedra may be determined in the same way by allowing the pairs AC and BD or AD and BC to play the role previously assigned to AB and CD. That is, e.g., define $R_1' = \overline{AC}$, $R_2' = \overline{BD}$, place AC perpendicular to the line, z', joining its midpoint with that of BD, define R' as the distance between the midpoints, and select the dihedral angle between the plane contining AC and z' and the plane containing BD and z' to be 90°. This results in a tetrahedron (AC, BD). Similarly, R_1'', R_2'', and R'' refer to a tetrahedron (AD, BC). Because the four nuclei are equivalent, the energy surfaces for tetrahedra (AC, BD) and (AD, BC) look just like those shown in Figures 2–5 for (AB, CD), except that the axes are labeled differently. The

three sets of surfaces are conveniently distinguished by imagining them to be colored red, white, and blue, respectively. Namely, the red surfaces, for the (AB, CD) tetrahedra, have $R_1 = \overline{AB}$, $R_2 = \overline{CD}$, and R as the distance between midpoints of AB and CD as discussed above. The white surfaces, for the (AC, BD) tetrahedra, have $R_1' = \overline{AC}$, $R_2' = \overline{BD}$ and R' as the distance between midpoints of AC and BD. The blue surfaces, for the (AD, BC) tetrahedra, have $R_1'' = \overline{AD}$, $R_2'' = \overline{BC}$, and R'' as the distance between midpoints of AD and BC.

All three spaces have the line of regular tetrahedra in common, since here the three pairs of sides simultaneously satisfy the triply right condition. A given regular tetrahedron, ABCD, can be distorted by holding AB and CD perpendicular to the line joining their midpoints, thus moving into the red surfaces by increasing or decreasing the distance between AB and CD. Alternatively, AC and BD can be held perpendicular to the line joining their midpoints, thus moving into the white surfaces. Finally, AD and BC can be held perpendicular to the line joining their midpoints, thus moving into the blue surfaces.

The lowest singlet states in the subspace of triply right tetrahedra can be expected to be formed from the combinations of two hydrogen molecules in their low-lying states, $X^1\Sigma_g^+$ (ground), $b^3\Sigma_u^+$ (triplet), $B^1\Sigma_u^+$ (singlet excited). For brevity, we shall refer to these as the X, b, and B states of H_2. Several additional states follow closely, in particular $C^1\Pi_u$, . . . , and $E^1\Sigma_g^+$ (doubly excited). Of these, only the E state can be described at all with a minimum basis set. Since we shall find that it correlates with some low-energy states at geometries of H_4 of interest to us, we shall include it in the present consideration, although its description in terms of minimum basis set is rather inadequate. Results obtained with larger basis sets show that the other states (C, D) do not correlate with low-lying states of H_4 at square geometries.

The zero-order states which result for H_4 upon combination of the AB and CD H_2 molecules (C_{2v} symmetry group) are $X_{AB}\cdot X_{CD}$ (A_1), $b_{AB}\cdot b_{CD}$ (A_2), $X_{AB}\cdot B_{CD}$ (B_2), $B_{AB}\cdot X_{CD}$ (B_1), $X_{AB}\cdot E_{CD}$ (A_1), $E_{AB}\cdot X_{CD}$ (A_1). At D_{2d} geometries, the $X_{AB}\cdot X_{CD}$ remains A_1, A_2 becomes B_1, while B_1 and B_2 become the two degenerate components of an E representation, $X_{AB}\cdot E_{CD} + E_{AB}\cdot X_{CD}$ is A_1 and $X_{AB}\cdot E_{CD} - E_{AB}\cdot X_{CD}$ is B_2. At T_d geometries, the $X_{AB}\cdot X_{CD}$ and the B_1 states of D_{2d} become the components of the E representation, while the $X_{AB}\cdot E_{CD} + E_{AB}\cdot X_{CD}$ remains A_1 and the E and B_2 states of become T_1.

Figures 2–5 depict results for the four lowest singlet states S_0–S_3 within the space of triply right tetrahedra. The S_0 and S_1 surfaces touch and consist of the lowest A_1 and A_2 surfaces which cross. The S_2 and S_3 surfaces also touch and consist of the lowest B_2 and second lowest A_1 states which cross, at least within the prism shown in the figures. The continuation of the S_2 and S_3 surfaces (not shown), obtained by mirror reflection in the $R_1 = R_2$ plane, are formed by the lowest B_1 and second lowest A_1 states which cross. Due to the allowed crossing of hypersurfaces having different symmetries, the ground state S_0, first excited state S_1, etc., show discontinuities in the slopes of their potential surfaces at points where the different symmetry states change order. We do not depict the smooth energy surfaces belonging to pure symmetry states of the triply right tetrahedra, although it might seem more natural. As soon as the point group symmetry is lowered sufficiently and the crossings avoided, it is the S_0, S_1, etc., surfaces which correspond with successive states of the distorted tetrahedra. For example, by rotating both H_2 molecules, AB and CD, through the angle $\alpha/2$ in opposite directions about the line joining their midpoints (z) one moves from the present triply right tetrahedron ($\alpha = 90°$) through doubly right tetrahedra ($0 < \alpha < 90°$) to the planar trapezoids ($\alpha = 0°$) of part I.[2] The doubly right tetrahedra have, in general, C_2 symmetry, so that A_1 and A_2 representations of C_{2v} both become A, while B_1 and B_2 both become B and some crossings are avoided; some discontinuities then become smoothed as the dihedral angle departs from $\alpha = 90°$. Hence, there is a gradual evolution of the present surfaces through those corresponding to all doubly right tetrahedra and ultimately into those corresponding to the trapezoids of part I.

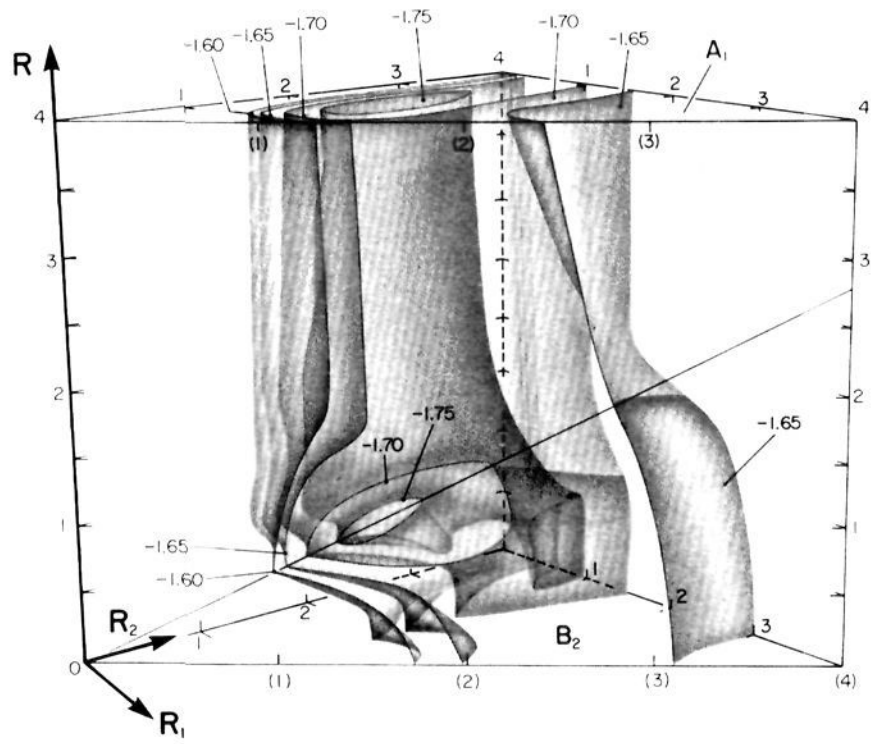

Figure 5. The third excited singlet, S_3, potential energy hypersurfaces of triply right tetrahedral H_4.

States Correlating with the E State of Regular H_4 Tetrahedra

The Ground State, S_0. The "red" set of isoenergetic surfaces for the ground state of (AB, CD) tetrahedra is depicted in Figure 2.

(i) The Vertical Tube. The low-energy tube at the upper left (R large and $R_1 = R_2 \sim 0.76$ Å) represents two distant H_2 molecules AB and CD oriented as shown in Figure 1, each in its ground state ($X^1\Sigma_g^+$). In this region, the symmetry of the S_0 state is A_1 in the C_{2v} group. The energy in the tube is lowest (−2.293 au) at $R = \infty$. If R_1 and R_2 are kept equal as R decreases, the energy increases very slowly until the separation reaches about 1.5 Å. Then, it begins to climb steeply. If R_1 and R_2 are permitted to differ as R decreases, the energy increases more slowly. The difference is insignificant at large values of R, but becomes overwhelming when R reaches less than about 1.5 Å; cf. the cross sections in Figures 6 (R = 2 Å), 7 (R = 1 Å), and 8 (R = 0). At any value of R, it is easier to increase only R_1 or only R_2 from their optimum values than to increase both, and this accounts for the wings which protrude from the center of the tube toward the cracks which are clearly seen in Figure 2 at large R and in Figure 6. Motion from the center of the tube into one of the cracks corresponds to the dissociation of one of the H_2 molecules. This is quite difficult at large values of R and requires 0.148 au (93 kcal/mol). As R decreases and the energy in the center of the tube increases, this dissociation becomes easier (about 0.1 au at R = 1.5 Å, and 0 au at $R \sim$ 1.25 Å) and eventually exothermic (Figures 7 and 8). Thus, if motion down the tube is forced, the least-energy escape path corresponds to dissociation of one of the H_2 molecules well before R reaches zero. If one is only willing to expend the minimum amount of energy and yet proceed all the way to R = 0, it is not possible to keep the two dissociated H atoms closer than about 3 Å apart at best. Thus, an attempt to move one ground-state H_2 bond through another in perpendicular orientations results in complete dissociation of one of them.

(ii) The Square Minimum. The minimum at the geometry of a 1.42-Å square, seen as a quarter-bubble in the lower front

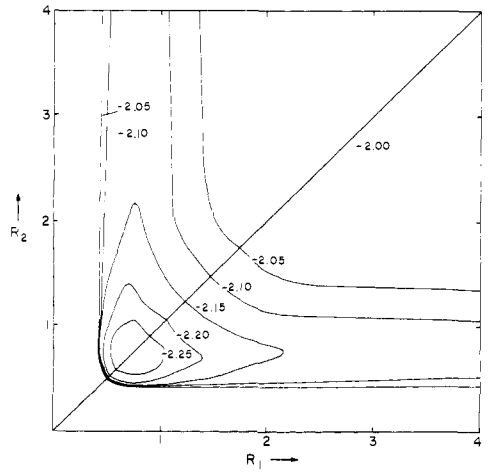

Figure 6. Potential energy (in au) contours of the S_0 state on the cross section through Figure 2 at $R = 2$ Å.

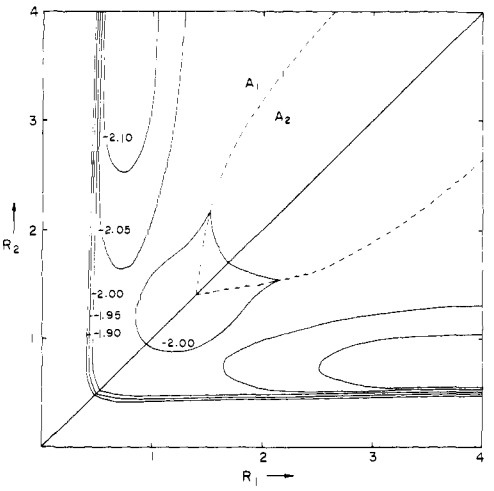

Figure 7. Potential energy contours of the S_0 state on the cross section through Figure 2 at $R = 1$ Å.

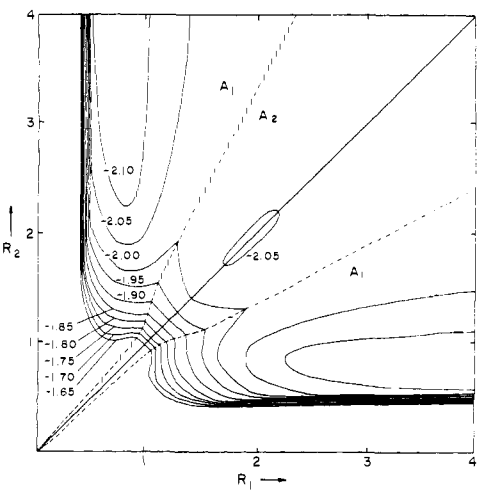

Figure 8. Potential energy contours of the S_0 state on the cross section through Figure 2 at $R = 0$ Å, planar geometries.

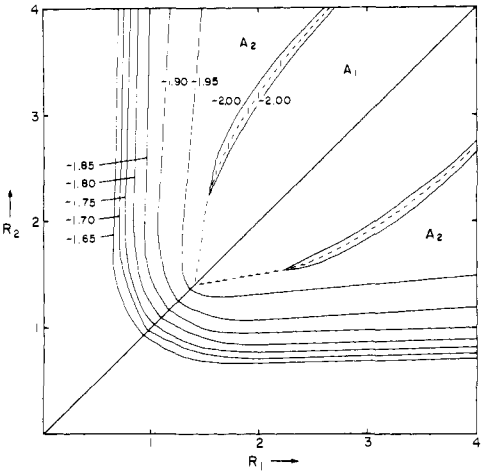

Figure 9. Potential energy contours of the S_1 state on the cross section through Figure 3 at $R = 1.0$ Å.

of Figure 2, occurs at rather high energy (−2.058 au) and is familiar from part I. It is a saddle point with respect to trapezoidal distortions discussed in part I. The symmetry of S_0 at this geometry is A_2 in the C_{2v} symmetry group of the tetrahedra of our three-dimensional subspace. Dissociation into four H atoms requires only 0.06 au of energy and can be accomplished, for example, by increasing the size of the square (see part I). It takes only 0.02–0.03 au of energy to climb out of the square minimum and proceed in the $R = 0$ plane directly into the bottom of the crack discussed under (i), i.e., to push two opposite vertices of the square together and pull the other two apart, forming $H_2 + 2H$. The spacing of contour lines in Figure 2, 0.05 au, does not display any information about the best path for this transformation, which has not been investigated in detail.

Motion from the square minimum toward larger R values in the front plane ($R_1 = R_2$) corresponds to pulling the two diagonals of the square apart. Along these paths, energy rises above −2.0 au before a T_d geometry is reached. Thus, motion from the square minimum to the vertical tube in the front plane is most economically achieved by total fragmentation to 4 H atoms followed by their recombination.

(iii) **The Surface of S_0–S_1 Touching.** The upper left region of the space shown in Figure 2, in which the symmetry of S_0 is A_1, is separated from the bottom right region, in which the symmetry of S_0 is A_2, by a curved surface which contains all points in which the S_0 and S_1 states touch (are degenerate). At the line of regular T_d tetrahedra, the A_1 and A_2 states form the two components of an E representation. The isoenergetic surfaces of S_0 (and S_1) states of Figure 2 (and 3) exhibit discontinuities in their derivatives where they meet the surface of S_0–S_1 touching. The lines of cross section of this surface with the planes $R = 0$, 1, and 2 Å are shown as dashed lines in Figures 6–8. The surface cuts the front plane ($R_1 = R_2$) in the line of regular tetrahedra (T_d) drawn in full in Figures 2 and 3.

The First Excited Singlet State, S_1. The "red" set of isoenergetic surfaces for the first excited singlet state, S_1 of (AB, CD) tetrahedra is shown in Figure 3. Departing from the surface of S_0–S_1 touching removes the degeneracy of S_0 and S_1, and S_1 follows the higher energy branch. In the upper left region in Figure 3 it has A_2 symmetry and in the lower right region it has A_1 symmetry. In order to imagine the shape of the isoenergetic surfaces for the A_2 state, one can imagine the prisms of Figures 2 and 3 to be solids, cleave them along the surface of S_0–S_1 touching, and combine the upper left of Figure 3 with the lower right of Figure. 2. For the A_1 state, one needs to combine the remaining sections (compare Figures 9 and 10 with Figures 7 and 8).

In the upper left section of Figure 3, where the S_1 state is of A_2 symmetry, the hypersurfaces represent the energy of two distant mutually perpendicular H_2 molecules, each in its $b^3\Sigma_u^+$ state, coupled into an overall singlet. This state is repulsive with respect to each H_2 and an energy profile along a line of con-

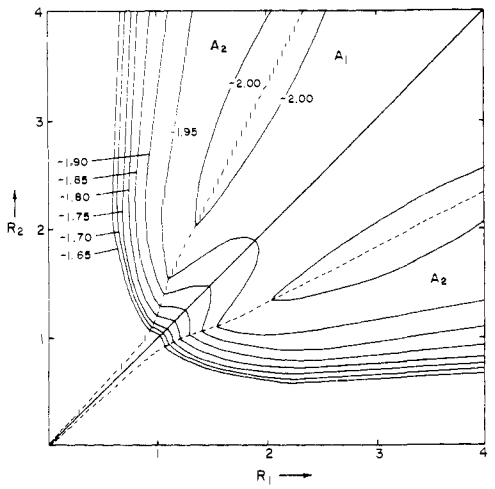

Figure 10. Potential energy contours of the S_1 state on the cross section through Figure 3 at $R = 0$ Å.

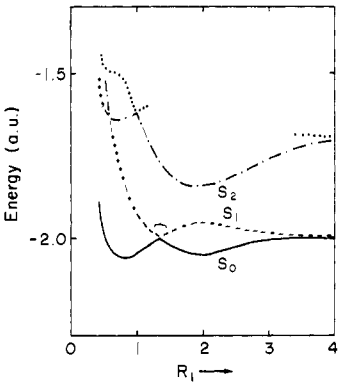

Figure 11. Profile of energy hypersurfaces through Figures 2, 3, and 4 on the line of constant $R = 0$, $R_2 = 2$ Å.

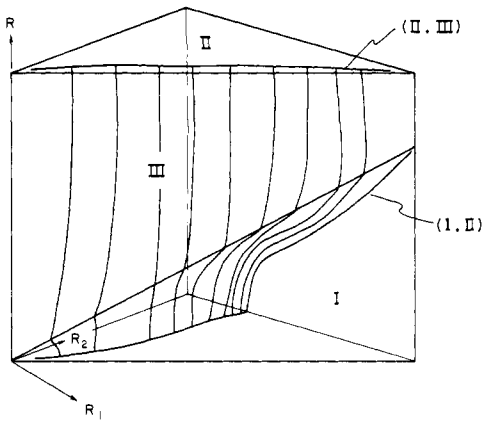

Figure 12. Schematic showing the partitioning of triply right tetrahedra H_4 geometries into regions with various orderings of states arising from the lowest T_1 state.

stant R_2 and R as a function of R_1 corresponds to the dissociation curve of triplet H_2 shifted up by the triplet energy of the other molecule. As R decreases, the energy profile is displaced to lower energies due to incipient singlet coupling between orbitals belonging to different molecules. As a result, the "triplet dissociation curve" of the energy profile dips below −2.0 au for values of R_2 around 1.5-2.5 Å (see Figure 11, which shows the energy profiles vs. R_1 with $R_2 = 2.0$ Å and $R = 0$). The fang shaped surface shown on the right of Figure 3 arises when the energy profile dips below −2.00 before it touches the S_0 surface (i.e., before the A_2 and A_1 surfaces cross); the thickness of this fang at $R = 0$, $R_2 = 2.0$ Å is about 0.1 Å and is depicted by the small horizontal brace in Figure 11.

The S_1 and S_2 energy hypersurfaces also touch in the upper left section of Figure 3. This touching is shown in the extreme upper portion of the S_1 profile of Figure 11, but has been omitted in Figure 3.

In the lower right section of Figure 3, where the S_1 state is of A_1 symmetry, it represents two stretched triplet H_2 molecules lying approximately side by side in the shape of a distorted square. The energy slopes downhill toward larger squares and also toward the surface of S_0-S_1 touching. Although we have not attempted to locate the geometry of minimum energy on S_1, it clearly lies within the fang-like surface of Figure 3 and its energy is between −2.00 and −2.05 au in our approximation. This minimum does not, however, represent a bound species. First, the energy may decrease upon distortion from the subspace of triply right tetrahedra; second, each time the molecular geometry crosses the surface of S_0-S_1 touching, the electronic state will switch from S_1 to S_0 (or from S_0 to S_1); i.e., the symmetry label will remain unchanged, either A_1 or A_2. At each point of the S_0-S_1 touching surface there is a hole ("funnel" [3]) in the S_1 hypersurface, efficiently returning excited molecules to the S_0 ground state. In the usual representation of the type shown in Figure 11, the geometry of the funnel would appear to correspond to a point. Consideration of our results for the subspace of all triply right tetrahedra shows that the structure of a funnel can be much more complicated. Thus far, the "space of the funnel" is seen to be a two-dimensional surface rather than a single point. However, in the complete six-dimensional nuclear configuration space of H_4 the "space of the funnel" is found to be three-dimensional, since distortion of either angle θ_1 or angle θ_2 (but not both) from 90° (Figure 1) does not cause the symmetry species of A_1 and A_2 of the C_{2v} group to become identical and thus does not remove the S_0-S_1 touching. Since either θ_1 or θ_2 can be varied, there are actually two three-dimensional "funnel spaces", one green and one yellow (in the sense of part I), which share the two-dimensional surface discussed presently. The "bottom" of the funnel may lie somewhere on this two-dimensional surface, or else, the funnel is double and has one "bottom" in the green and one in the yellow three-dimensional "funnel spaces". Consideration of more than one octant in our RR_1R_2 subspace and more than one color (red, blue, white) multiplies the number of possible "bottoms" related by symmetry.

States Correlating with the T_1 State of Regular H_4 Tetrahedra

The three states, $X_{AB}{\cdot}B_{CD}$ (B_2), $B_{AB}{\cdot}X_{CD}$ (B_1), and the out-of-phase combination of $X_{AB}{\cdot}E_{CD}$ and $E_{AB}{\cdot}X_{CD}$ (A_1) (all labeled in C_{2v} group) all become degenerate at the line of regular tetrahedra (Figures 4 and 5). The subspace of triply right tetrahedra is divided into three sections, I, II, and III, by surfaces at which S_2 and S_3 are degenerate (Figure 12). These surfaces of crossing all meet at the line of regular tetrahedra. The first of them is the $R_1 = R_2$ plane, the next two are curved. One (I, II) separates sections I and II. It proceeds from the line of regular tetrahedra behind and below and cuts the bottom plane of the prism ($R = 0$) in the dashed line shown in Figure 13 (cf. the discontinuities in Figures 4 and 5). Its intersection with the $R = 1$ Å plane is shown in Figure 14. The last surface (II, III) separates section II from section III and runs from the line of regular tetrahedra up close to the $R_1 = R_2$ plane. It is not shown in Figures 4 and 5. In region I, the order of state energies is $E(A_1) < E(B_2) < E(B_1)$. In region II, the order is $E(B_2) < E(A_1) < E(B_1)$. In region III, it is $E(B_2) < E(B_1) < E(A_1)$. In the front prism formed by reflection in the $R_1 = R_2$

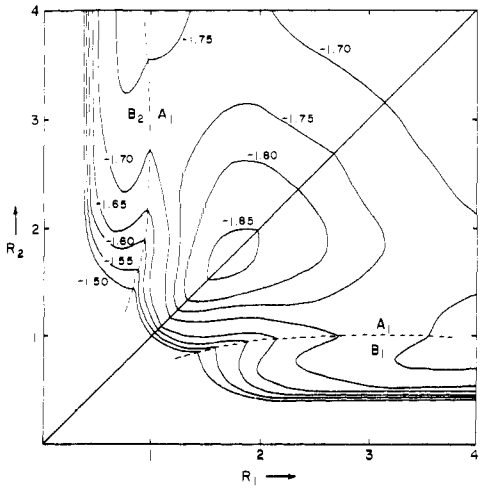

Figure 13. Potential energy contours of the S_2 state on the cross section through Figure 4 at R = 0 Å.

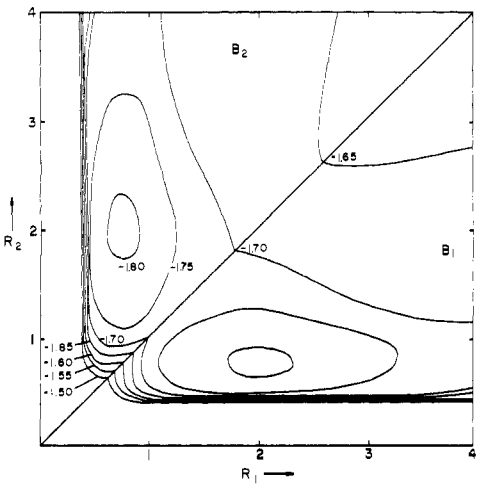

Figure 15. Potential energy contours of the S_2 state on the cross section through Figure 4 at R = 4.00 Å.

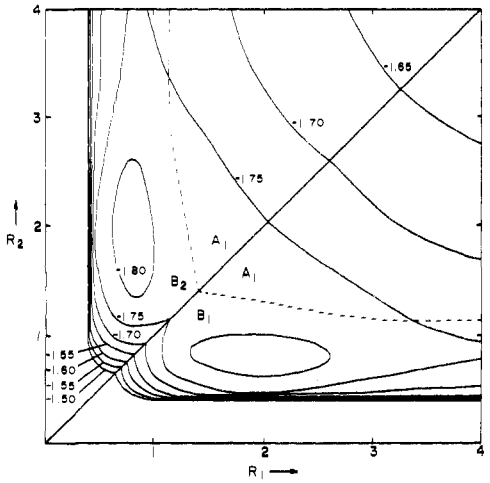

Figure 14. Potential energy contours of the S_2 state on the cross section through Figure 4 at R = 1.0 Å.

plane mirror image regions I′, II′, and III′ exist. The state ordering in these is the same, except that B_1 and B_2 labels are interchanged.

In the $R_1 = R_2$ plane, $E(B_2) = E(B_1)$. In each region, the lowest of the three states is S_2, the next S_3, and the highest S_4. Figure 4 shows the isoenergetic surfaces for S_2, Figure 5 shows the surfaces for S_3, except that the surfaces for A_1 were continued from region II into the very narrow region III for clarity, although those for B_1 should have strictly been used.

The Second Excited Singlet State, S_2. The "red" set of isoenergetic surfaces for the second excited state, S_2, of (AB, CD) tetrahedra is shown in Figure 4.

(i) **The Vertical Tube.** In region II of Figure 4, where the symmetry is B_2, there is a conspicuous tube entering the prism at R = 4, $R_1 \simeq 0.76$, and $R_2 \simeq 2.0$ Å, corresponding to the approach of one H_2 molecule (AB) in the ground state, $X^1\Sigma_g^+$, toward another (CD) in the excited state $B^1\Sigma_u^+$. Unlike a similar approach of two ground state molecules (Figure 2), this approach is slightly attractive and leads toward the minimum, enveloped by the −1.80 contour, at about −1.82 au near R = 1.5 and R_1 = 1.0, R_2 = 1.9 Å. Thus, the −1.80 surface forms a long narrow neck and body of an amphora ending near R = 1.0 Å. This amphora lies at the left end of a vertical crack parallel to the RR_2 plane. Higher energy contour surfaces, such as E = −1.75 au, grow very large near the end of the bottle and cross the $R_1 = R_2$ mirror plane into the front half of the prism (not shown), where they continue around the mirror image amphora describing an approach of (AB) $B^1\Sigma_u^+$ toward (CD) $X^1\Sigma_g^+$. The minima at the ends of these tubes in the space of triply right tetrahedra do not represent true minima in the full molecular configuration space. They probably connect without activation with the H_4 excimer state by decrease in the dihedral angle α, leading to a trapezoid in which the two original H_2 molecules lie side by side.[4] Another way of forming a trapezoid, in which the two original H_2 molecules now lie across each other, is to decrease R, keeping constant R_1 and R_2, until a rhombus is formed, and to distort the rhombus in plane into a square in the space of triply right tetrahedra,[5] and eventually, into a trapezoid. This second path proceeds across an energy barrier discussed below.

If R_1 and R_2 are allowed to relax while R is decreased beyond the bottom of the amphora, R_2 rapidly becomes longer, while R_1 decreases slightly to 0.76 Å (Figures 13–15). This process leads to a narrow rhombus when R = 0 is reached. This rhombus corresponds to a local minimum in the R = 0 plane, which is not seen in Figures 4 nor 13, since it occurs at $R_2 >$ 4 Å. This part of the subspace was not investigated in detail, since Rydberg states, which are not described with our basis set, will clearly intervene at these geometries. Overall, a descent into the amphora followed by further decrease of R and increase of R_2 corresponds to a dissociation of an excited H_2 molecule toward a weakly bound complex in which H^+ is separated by ground state H_2 from H^-, as a result of a "crossed" collision with a ground state H_2 molecule. Regardless of this complication, we see that an attempt to move an excited H_2 bond through a ground state H_2 bond in perpendicular orientation results in a nearly complete or perhaps complete dissociation of the excited bond, in close analogy to the situation found earlier with bonds in the ground state.

(ii) **The Square Minimum.** In region I of Figure 4, where the symmetry of the S_2 state is A_1 (under the C_{2v} group), there is a minimum at a square geometry having sides close to 1.27 Å (diagonals $R_1 = R_2$ = 1.80 Å) and energy E = −1.861 au. This minimum is familiar from part I[2] and lies very near the best trapezoidal geometry as well as the best kite geometry.[6] The easiest uphill escape in the subspace of triply right tetrahedra lies in the $R_1 = R_2$ plane and proceeds toward a tetrahedral geometry (front of Figure 4), about 60 kcal/mol uphill, where the top of the barrier is reached. Descent into the "amphora" follows and results in a gain of about 35 kcal/mol. The easiest escape from the square minimum confined to the R = 0 plane proceeds toward a narrow rhombus corresponding to a ground state H_2 molecule and an H^+H^- ion pair. Again, consideration of Rydberg states would change this.

(iii) **The Front Prism.** As mentioned in the introduction, the

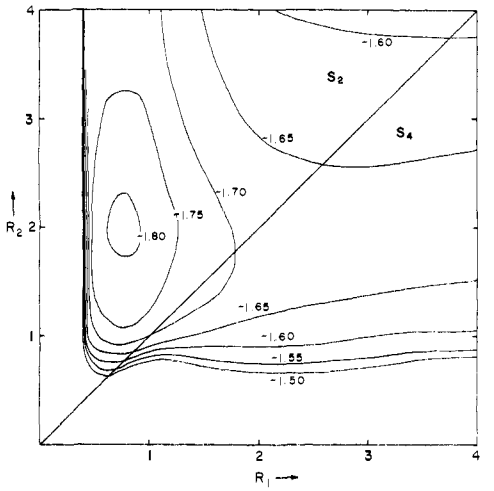

Figure 16. Potential energy contours for the B_2 state on a plane of $R = 4.00$ Å. The B_1 state contours are generated by mirror reflection in the $R_1 = R_2$ line.

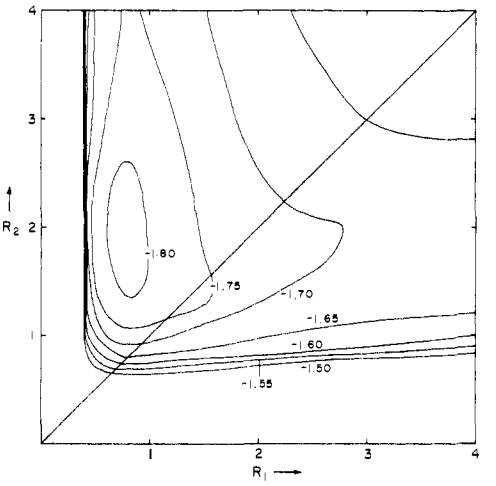

Figure 17. Potential energy contours for the B_2 state on a plane of $R = 1.00$ Å. The B_1 state contours are generated by mirror reflection in the $R_1 = R_2$ line.

isoenergetic surfaces S_0–S_3 shown in Figures 2–5 continue into the prism which lies in front of the $R_1 = R_2$ plane and can be obtained by mirroring in this plane. While at geometries in regions II and III of Figure 4 the S_2 state is of B_2 symmetry, at mirror image geometries in the front prism it is of B_1 symmetry. However, the isoenergetic surfaces of the B_2 state also continue smoothly across the $R_1 = R_2$ plane into the front prism (not shown in Figure 4), as is clear from the cross sections shown in Figures 16 and 17, which show energy contours for the B_2 state regardless of whether it represents S_2, S_3, S_4, or an even higher singlet state. A mirror reflection of the contours shown for the B_2 state in the section where $R_1 > R_2$ across the $R_1 = R_2$ plane back into the region $R_2 > R_1$, shown as the prism in Figures 2–5, would then give information about the B_1 state in this prism, where it represents S_3, S_4, or even higher states, but these results are not shown. The mirroring of unsymmetrical contours of the type shown in Figures 16 and 17, relating the B_2 and B_1 states, clearly produces a double degeneracy in the $R_1 = R_2$ plane, where B_1 and B_2 form an E representation of the D_{2d} group.

The Third Excited Singlet State, S_3. The "red" set of isoenergetic surfaces for the third excited singlet state, S_3, of (AB, CD) tetrahedra is shown in Figure 5. In region I of the figure, where the state symmetry is B_2 (under C_{2v} group), they represent a smooth continuation of the sheets enveloping the amphora of the S_2 state. The "tube" broadens and rises gently in energy from the (I, II) surface toward the $R = 0$ plane, where it connects to mirror image surfaces which envelop a mirror image amphora in the prism below. The energy increases as the $R_1 = R_2$ plane is approached; at the same time, the energy of the next higher state B_1 (S_4) decreases, and the two become degenerate in the plane (E representation of the D_{2d} group). Somewhat lower in energy lies the previously discussed state S_2, which is of B_2 symmetry in the D_{2d} group (A_1 in the C_{2v} group) in the lower section of the $R_1 = R_2$ plane, where this plane adjoins region I. At the line of regular tetrahedra, this B_2 state becomes degenerate with the E state of the D_{2d} group, and jointly they form the T_1 representation of the T_d group. Above this line, where the $R_1 = R_2$ plane adjoins region III, the B_2 state of the D_{2d} group lies above the E state (Figure 18). In the narrow region III, close to the $R_1 = R_2$ plane, the S_3 state is then represented by the higher energy component (B_1) and the S_2 state by the lower energy component (B_2), which result when the E state of the D_{2d} group splits as symmetry is lowered upon leaving the $R_1 = R_2$ plane. Since the B_1 state rapidly increases in energy as the distance from the $R_1 = R_2$ plane grows, it soon catches up with the A_1 state

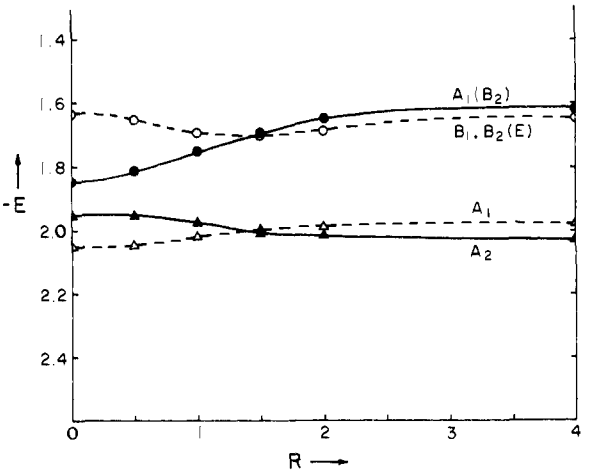

Figure 18. Profile of energy hypersurfaces vs. R (in Å) through Figures 2, 3, 4, and 5 on the line of constant $R_1 = R_2 = 2.00$ Å, showing the crossing of different symmetry states in the D_{2d} tetrahedra to produce the E and T_1 states of the regular tetrahedra. Labels refer to C_{2v} symmetry group (those in parentheses refer to D_{2d}).

(corresponding to the B_2 state of the D_{2d} group). This occurs at the crossing surface (II, III) shown in Figure 12, but not apparent in Figure 5. Thereafter, in region II, the third excited singlet state S_3 has A_1 symmetry. The discontinuity which should occur in the S_3 surfaces in Figure 5 upon crossing the (II, III) surface is not shown, since the visualization is too difficult, and the difference insignificant.

The shape of the S_3 isoenergetic surfaces in region II (A_1 symmetry) is similar to that of the S_2 surface (Figure 5). The vertical tube corresponds to the approach of one H_2 molecule (AB) in the ground state, $X^1\Sigma_g^+$, toward another (CD) in the doubly excited state $E^1\Sigma_g^+$. Since the E state is described very poorly in the minimum basis set, no importance can be attached to the details of the shapes. The one significant feature is the downhill slope with decreasing R, due to correlation of the A_1 state with the "excimer" state at square geometries of part II. Because of the crossing of the S_2 and S_3 surfaces at the (I, II) surface, the downhill slope in S_3 in region II continues downward in Figure 5 only until this surface is reached, similarly as its downhill slope in region I continued upward only until the same surface was reached. Similarly as was the case for the surfaces S_0 and S_1, the crossing of the A_1 and B_2 states then forms a "ridge" in the S_2 surface and a "funnel" in the S_3 surface. The points of this funnel form a two-dimensional

surface in the subspace of triply right tetrahedra, but in the full six-dimensional space of H_4 the funnel again consists of two three-dimensional "funnel spaces" which share the two-dimensional surface (I, II). At T_d geometries, additional complications arise due to the third component of the T_1 state.

Discussion

Wave Functions. The VB wave function of the lowest A_1 state corresponds predominantly to a pair of covalent bonds A–B and C–D. Interactions A–C, A–D, B–C, and B–D are predominantly antibonding. As two 0.76-Å long H_2 molecules are brought together in a perpendicular arrangement, the latter interactions gradually increase and the energy rises. On the other hand, the VB wave function of the lowest A_2 state contains net A–B and C–D antibonding and net A–C, A–D, B–C, and B–D bonding, and this state correlates with two triplet H_2 molecules A–B and C–D. Its energy decreases as the two H_2 molecules approach, since the bonding interactions are strengthened. When the geometry of a regular tetrahedron is reached, the bonding and antibonding interactions in A_1 and A_2 approximately balance and both states are degenerate. As the tetrahedron is flattened further, until finally a square is reached, the antibonding peripheral interactions A–C, A–D, B–C, and B–D in the A_1 state prevail over the bonding diagonal interactions A–B and C–D and the D state of the square discussed in part I[2] is reached. At the same time, the bonding peripheral interactions in the A_2 state prevail over the antibonding diagonal interactions and the lower G state of the square discussed in part I[2] is reached. This accounts in an intuitive manner for the shapes of the S_0 and S_1 surfaces, in particular for the reluctance of the two crossed H_2 molecules to proceed to the square geometry, for the tendency of the S_1 state to dissociate to H atoms (each triplet H_2 molecule is repulsive), for the existence of a local minimum in the S_0 state at square geometry, in the subspace of triply right tetrahedra, and for the ease with which the S_1 state at square geometry distorts toward a tetrahedron. The very weakly bonded "fang" in the S_1 surface appears to be due to slight domination of peripheral bonding over diagonal antibonding if the diagonals are long enough.

The VB wave function of the B_2 and B_1 states corresponds predominantly to a combination of a ground state with a singly excited (zwitterionic) H_2 molecule. In the former, the excitation resides on the longer molecule; in the latter, on the shorter one. At small R_1 and R_2, it is better to place excitation on the longer molecule and B_2 lies below B_1. The situation is reversed for larger values of R_1 and R_2. This is easily understood: once the ground state H_2 molecule is about completely dissociated, its length has very little effect on its energy. At these lengths, the longer excited H_2 molecule is still far from dissociated and making it shorter and thus closer to equilibrium bond length saves energy.

When an H_4 system in its S_2 state proceeds down the "amphora", energy decreases by about 5 kcal/mol. This can be attributed to contributions from charge-transfer structures in which an electron is transferred from the shorter to the longer H_2 molecule. In the perpendicular approach, there is no stabilization by exciton splitting as there was in the trapezoidal approach of part I;[2] there, the stabilization was much larger (26 kcal/mol). When the distance of the two crossed interacting molecules is decreased beyond 1.5 Å or so, the energy increases steeply, mostly due to electron–electron repulsion.

The A_1 state, corresponding to a doubly excited H_2 molecule interacting with a ground H_2 molecule, is represented by very similar zwitterionic VB structures as the B_2 state. However, its symmetry allows it to correlate directly with the energetically favorable excimer state at square geometries, so that it crosses the B_2 state at the geometry of a regular tetrahedron and becomes the S_2 state. As the square geometries are approached, there is an interaction of the zero-order zwitterionic A_1 wave function of this excited state with the zero-order covalent A_1 wave function of the S_1 state, resulting in considerable admixture of ionic character into the latter in accordance with the discussion in part I.[2]

Symmetry Breaking. As pointed out in the section, Method of Calculation, at D_{2d}, D_{4h}, or T_d geometries the full CI solutions in the minimum basis set frequently do not possess irreducible symmetry of the group when full freedom is allowed for orbital exponent optimization (exponents of A and B orbitals are different from those of C and D orbitals). Such "symmetry breaking" for a constrained wave function is well known in SCF calculations, but has not been previously observed for full CI calculations as far as we are aware. We believe that the physical reasons for the symmetry breaking in our case are the great energy difference between a single ζ and double ζ level of approximation to the true wave function, the closeness of two states of appropriate irreducible symmetries, and the similarity of their optimized double ζ exponents. The occurrence of symmetry breaking implies that the average energy of the two symmetry-adapted components which can be projected out of the broken symmetry solution, and which represent double ζ approximations to the lowest two states of appropriate irreducible symmetries, lies below the single ζ approximation to the lower of these states. The broken symmetry exponents can be said to be optimized for neither of the two symmetry-adapted components separately, but represent the best compromise choice for both states simultaneously at the double ζ level. Therefore, when the separately fully optimized double ζ exponents for the two states in question lie close to each other, symmetry breaking at the single ζ level is favored.

Photochemical Processes in H_4. Until more of the six-dimensional space of H_4 is mapped out, it is difficult to make predictions for the course of photochemical reactions involving this system. Nevertheless, the present results, combined with those obtained in part I for excimer formation, strongly suggest a rationalization of the observed[7,8] efficient quenching of excited ($B^1\Sigma_u^+$) H_2 by ground state H_2. As discussed in part I, it appears most likely that an excimer H_4*, a species in the second excited singlet state of H_4, is formed first. Internal conversion into the almost degenerate lowest excited singlet S_1 could be efficient. A dissociation of square H_4 in the S_1 state into 4 H by increasing the square size appears possible and was already discussed in part I. The present results suggest an even more facile path, namely return to S_0 through the "funnel" of S_0–S_1 touching. Because of the large dimensionality of the funnel already discussed above, this could occur along a variety of paths which all involve diagonal bonding in the square H_4 array. The likely products are either $H_2 + 2H$, or $H_2 + H_2$. It is, of course, possible that the H_2 formed might be so hot as to further dissociate into 2H. At any rate, one only needs to postulate a rapid conversion of the S_2 excimer to the almost degenerate S_1 state and an efficient mechanism for loss of electronic excitation by the latter becomes available.

Extrapolation to Larger Molecules. While details of the shape of potential energy hypersurfaces for H_4 are clearly not transferable to other four-electron four-orbital systems, there is little doubt that the propensity for diagonal bonding in the S_1 state of a pericyclic array of $4N$ interacting AO's containing four electrons, due to a (possibly avoided) correlation of the S_1 state with S_0 state of the product along this path, is independent of the exact nature of the system. This then suggests that molecules which find themselves in the pericyclic minimum in the S_1 surface, discussed in detail for the first time by van der Lugt and Oosterhoff[9] and more recently in part I,[2] can not only decay to S_0 at the cyclic geometry and subsequently proceed to the ordinary 2s + 2s product, but, in competition to this process, could also first establish diagonal bonding in

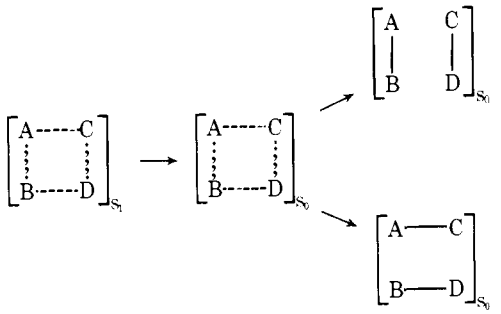

the S_1 state if this is sterically feasible. Such a change in geometry takes them to the "cross-bonding" funnel investigated in this paper. Perhaps more important, the "cross-bonding" funnel might be accessible from starting points other than a $4N$ pericyclic array, at which competing $S_1 \rightarrow S_0$ return to the ground state probably is quite efficient. In the present highly symmetrical case, the S_0 and S_1 states actually touched at the

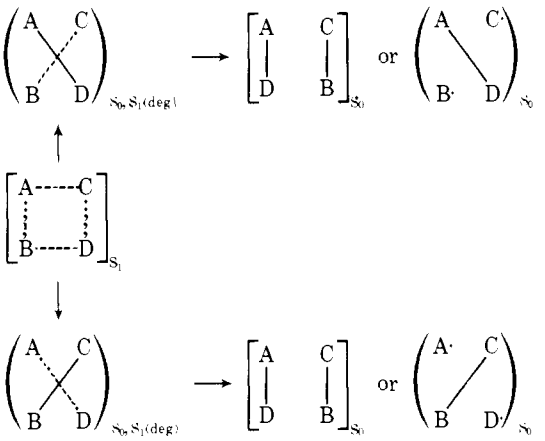

funnel geometry, so that return to S_0 would be fully efficient (the return to S_0 occurs as soon as the funnel is reached). In more typical cases of lower symmetry, the touching will usually be avoided, but the same type of products ought to result. For example, starting with the s-cis conformer of 1,3-butadiene (I),

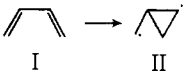

I II

formation of 1,3-biradicals of the type II appears quite plausible. The ultimate fate of the biradicals might be return to the starting material or to its cis-trans isomer, formation of a bicyclobutane, methylenecyclopropane, or methylcyclopropene. At this time, this proposal is rather speculative. Products of this type are well known to result from irradiation of dienes, but are usually believed and in many cases known[10,11] to originate in the s-trans conformer of the diene. A different mechanism involving twisting around one of the terminal C=C bonds has been proposed for their formation.[10,12] A more recent alternative suggestion,[13] that the excited s-trans conformer of the diene (III) twists around its 2,3 bond and relaxes into a ge-

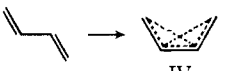

III IV

ometry with two 1,3 overlaps (IV) similar to our "cross-bonding" funnel geometry, where it presumably returns to the S_0 surface to produce a bicyclobutane and/or cyclopropenes, is more in line with the present arguments. Our results indicate in simple terms why such a "cross-bonding" or "tetrahedral" geometry ought to be energetically favorable in the S_1 state and why it should return the molecule rapidly to the S_0 state. However, no definitive conclusions can be drawn at this time, and before we can profitably discuss the nature of the photochemical processes for the s-trans isomer, additional subspaces of H_4 need to be mapped (parallelograms, etc.). Note also that the present model only allows us to analyze the case of disrotatory ring closures. It is likely, however, that an even number of conrotations would not change the results.

In summary, then, the present results for the subspace of triply right tetrahedra of H_4 suggest some possibilities for analogous processes in larger molecules, but additional work is clearly required.

Acknowledgment. Support of this work by the National Science Foundation (GP-37551) and by grants of computer time received from the Research Committee of the University of Utah and from Washington State University are gratefully acknowledged. One of us (W.G.) expresses his thanks to NATO for a postdoctoral fellowship.

References and Notes

(1) (a) NATO Postdoctoral Fellow; (b) University of Utah; (c) Washington State University.
(2) W. Gerhartz, R. D. Poshusta, and J. Michl, *J. Am. Chem. Soc.*, **98**, 6427 (1976).
(3) J. Michl, *Mol. Photochem.*, **4**, 243, 257 (1972); *Top. Curr. Chem.*, **46**, 1 (1974); *Pure Appl. Chem.*, **41**, 507 (1975).
(4) This trapezoidal geometry lies in the "red space" of part I.
(5) This square geometry lies in the red space of triply right tetrahedra at the line of $R_1 = R_2$, $R = 0$ in the lower center of Figure 4. At the same time it lies in the intersections of the blue and white trapezoidal subspaces of part I.
(6) J. Michl and R. D. Poshusta in "The Exciplex", M. Gordon and W. R. Ware, Ed., Academic Press, New York, N.Y., 1975, p 145.
(7) E. H. Fink, D. L. Akins, and C. B. Moore, *J. Chem. Phys.*, **56**, 900 (1972); E. H. Fink, P. Hafner, and K. H. Becker, *Z. Naturforsch. A*, **29**, 194 (1974).
(8) I. N. Knyazev, V. S. Letokhov, and V. G. Movshev, *IEEE J. Quantum Electron.*, **QE-11**, 805 (1975).
(9) W. Th. A. M. van der Lugt and L. J. Oosterhoff, *J. Am. Chem. Soc.*, **91**, 6042 (1969).
(10) W. G. Dauben and J. S. Ritscher, *J. Am. Chem. Soc.*, **92**, 2925 (1970).
(11) R. B. Reinarz and G. J. Fonken, *Tetrahedron Lett.*, 441 (1974).
(12) V. Bonacic-Koutecký, P. Bruckmann, P. Hiberty, J. Koutecký, C. Leforestier, and L. Salem, *Angew. Chem., Int. Ed. Engl.*, **14**, 575 (1975).
(13) M. Bigwood and S. Boué, *J. Chem. Soc., Chem. Commun.*, 529 (1974).